ACS Energy LETTERS

Cite This: ACS Energy Lett. 2017, 2, 2805-2811

http://pubs.acs.org/journal/aelccp

LETTER

Intrinsic Lead Ion Emissions in Zero-Dimensional Cs_4PbBr_6 Nanocrystals

Jun Yin,[†] Yuhai Zhang,[†] Annalisa Bruno,[‡,⊥] Cesare Soci,[‡] Osman M. Bakr,[†] Jean-Luc Brédas,*[,§] and Omar F. Mohammed*[,†]

[†]KAUST Solar Center, Division of Physical Science and Engineering, King Abdullah University of Science and Technology, Thuwal 23955-6900, Kingdom of Saudi Arabia

[‡]Division of Physics and Applied Physics, School of Physical and Mathematical Sciences, Nanyang Technological University, 21 Nanyang Link, Singapore 637371

[§]School of Chemistry and Biochemistry, Center for Organic Photonics and Electronics (COPE), Georgia Institute of Technology, Atlanta, Georgia 30332-0400, United States

[⊥]Energy Research Institute @ Nanyang Technological University (ERI@N), 50 Nanyang Avenue, Singapore 639798

Supporting Information

ABSTRACT: We investigate the intrinsic lead ion (Pb^{2+}) emissions in zero-dimensional (0D) perovskite nanocrystals (NCs) using a combination of experimental and theoretical approaches. The temperature-dependent photoluminescence experiments for both "nonemissive" (highly suppressed green emission) and emissive (bright green emission) Cs_4PbBr_6 NCs show a splitting of emission spectra into high- and low-energy transitions in the ultraviolet (UV) spectral range. In the nonemissive case, we attribute the high-energy UV emission at approximately 350 nm to the allowed optical transition of $^3P_1$ to $^1S_0$ in Pb^{2+} ions and the low-energy UV emission at approximately 400 nm to the charge-transfer state involved in the 0D NC host lattice (D-state). In the emissive Cs_4PbBr_6 NCs, in addition to the broad UV emission, we demonstrate that energy transfer occurs from Pb^{2+} ions to green luminescent centers. The optical phonon modes in Cs_4PbBr_6 NCs can be assigned to both Pb−Br stretching and rocking motions from density functional theory calculations. Our results address the origin of the dual broadband Pb^{2+} ion emissions observed in Cs_4PbBr_6 NCs and provide insights into the mechanism of ionic exciton−optical phonon interactions in these 0D perovskites.

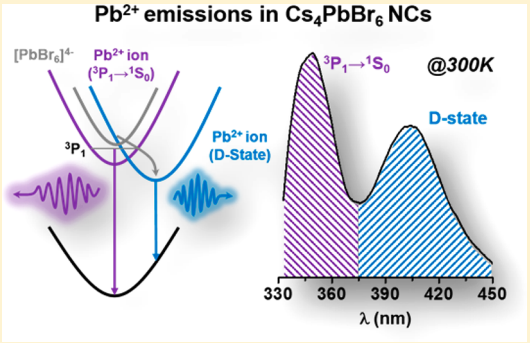

Metal-halide perovskites (MHPs) have attracted much attention over the past few years because of their promising applications in optoelectronic devices.[1−8] In these MHPs, the basic building block is an octahedral BX_6, where B is a metal and X is a halogen. The octahedral units can be arranged in different ways to form three-dimensional (3D), two-dimensional (2D), one-dimensional (1D), and even zero-dimensional (0D) crystal structures.[9−13] The 3D MHP[14−17] structures with a general formula of ABX_3 (A is an organic or inorganic cation with an extended network formed by the corner-sharing metal-halide octahedra) are the most extensively studied.[18−20] In 2D structures, the octahedra are connected in layered or corrugated sheets separated by long organic cations.[21−23] In 1D MHPs, the octahedral blocks assemble in a chain surrounded by organic cations.[24] Finally, in the 0D cases, the octahedra are completely isolated from each other and surrounded by inorganic or organic cations; this leads to strong quantum confinement and strong exciton−phonon interactions.[9] Specifically, the prototypical 0D building block, Cs_4PbX_6 (X = Cl, Br, or I)[25] is expected to exhibit interesting photophysical properties because of the complete isolation of the $[PbX_6]^{4-}$ octahedra that can cause exciton localization and self-trapping[26] as well as small-polaron generation upon photoexcitation (unpublished results).

The early work on Cs_4PbX_6 single crystals and thin films focused on their fundamental optical absorption and photoluminescence properties and attempted to distinguish their emission properties from those of "3D-like" structures.[27−33] These works have demonstrated that, unlike 3D and other low-dimensional perovskites, the main optical characteristics of Cs_4PbX_6 are determined by transitions between electronic states of the Pb^{2+} ions, and the observed broadband ultraviolet (UV) emission spectrum was ascribed to the radiative decay of a Frenkel exciton at Pb^{2+} sites.[28] Thus, high-energy emissions

Received: October 19, 2017
Accepted: November 6, 2017

DOI: 10.1021/acsenergylett.7b01026
ACS Energy Lett. 2017, 2, 2805−2811

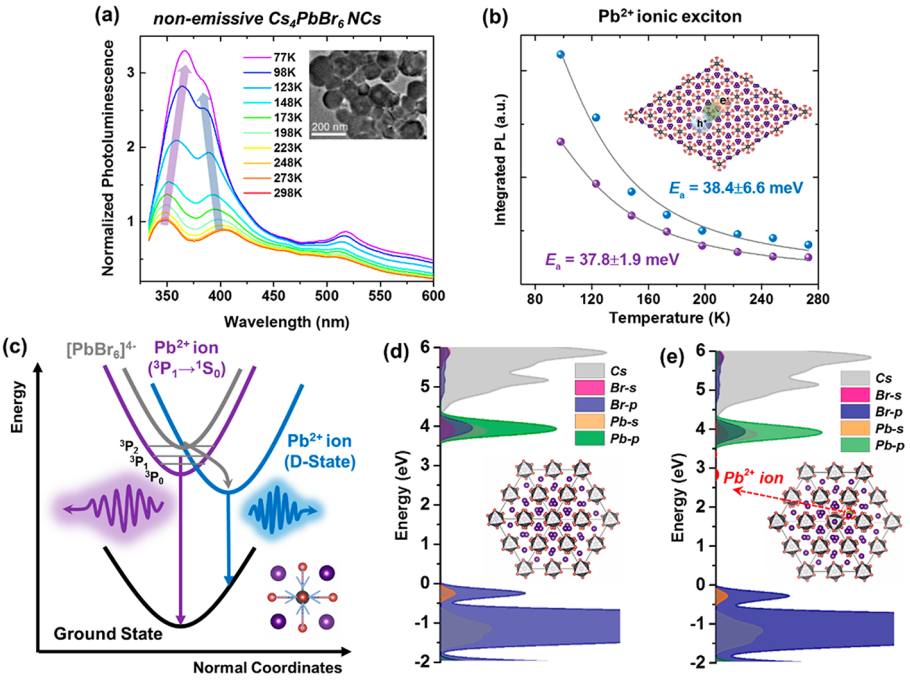

Figure 1. (a) Temperature-dependent steady-state photoluminescence spectra of nonemissive Cs_4PbBr_6 nanocrystals with the inset showing the TEM image; (b) temperature-dependent integrated PL intensity of high- and low-energy emission bands; (c) diagram of $^3P_1$ to $^1S_0$ and D-state emissions from Pb^{2+} ions; projected density of states of 2 × 2 × 2 Cs_4PbBr_6 supercells calculated at the PBE level of theory (d) before and (e) after the replacement of a Cs atom with a Pb^{2+} ion (the optimized crystal structures of the supercells are also given).

from Pb^{2+} ions become the main optical feature for 0D Cs_4PbX_6.

Recently, this basic understanding of the crystal structure and the optical properties of 0D Cs_4PbX_6 inspired many research groups to synthesize Cs_4PbX_6 nanocrystals (NCs) that are emissive in the visible (i.e., bright green luminescence) and "nonemissive" (i.e., strongly suppressed or vanishing green luminescence).[12,34−38] For example, we reported green-emissive colloidal Cs_4PbBr_6 NCs using a reverse microemulsion method, which have high photoluminescence quantum yield.[34,39] However, Akkerman et al. have recently found that Cs_4PbBr_6 NCs synthesized under Cs^+-rich reaction conditions have no green emission and that they can be converted into green fluorescent $CsPbBr_3$ NCs through a reaction with an excess of $PbBr_2$.[40] At the same time, Liu et al. have demonstrated the ligand-mediated transformation of presynthesized $CsPbBr_3$ NCs to Cs_4PbBr_6 NCs via the addition of an amine.[35] To clarify the green luminescent centers in emissive Cs_4PbBr_6 NCs, Quan et al. have proposed a model of lattice-matching between cubic $CsPbBr_3$ NCs and a Cs_4PbBr_6 matrix.[36] On the other hand, De Bastiani et al. have provided new insights into the origin of the green emissions in Cs_4PbBr_6 single crystals by ruling out any role of $CsPbBr_3$ nanocrystals or inclusion.[12] Despite the progress made on the understanding of green emission from Cs_4PbX_6 NCs, the intrinsic emission features of Cs_4PbX_6 NCs as well as how the Pb^{2+} ion emissions affect the luminescent centers in the emissive NCs remain unclear.

In this work, we study the intrinsic electronic behavior of both nonemissive and emissive in the green Cs_4PbBr_6 NCs by combining temperature-dependent photoluminescence experiments and density functional theory (DFT) calculations. For nonemissive Cs_4PbBr_6 NCs, our results show two broad UV emission spectra from Pb^{2+} ions with different origins. For emissive Cs_4PbBr_6 NCs, we show an energy transfer from Pb^{2+} ions to green luminescent centers, which can be significantly enhanced at high temperature because of the assistance of phonons. The relevant phonon modes of Cs_4PbBr_6 can be assigned via our DFT calculations to both Pb−Br rocking and stretching modes of each $[PbBr_6]^{4-}$ octahedron.

The nonemissive and emissive Cs_4PbBr_6 NCs were prepared by controlling the addition amount of oleic acid and oleylamine ligands (see Experimental Details in the Supporting Information). The X-ray diffraction (XRD) spectra of both samples are identical and confirm the zero-dimensionality of Cs_4PbBr_6 NCs (see Figure S1 in the Supporting Information). Both NCs have a uniform size of ∼120 nm as confirmed by the transmission electron microscopy (TEM) images (the insets in Figures 1a and 2a). The absorption spectra of both NCs can be found in Figure S2, showing the main absorption peak around 320 nm. It is notable that the absorption onset for emissive NCs at 510 nm is completely suppressed in the nonemissive case. Figure 1a shows the normalized photoluminescence of nonemissive NCs using a high excitation energy of 4.0 eV (above the bulk Cs_4PbBr_6 band gap of ∼3.9 eV). In addition to the significantly suppressed green emission at room temperature, the nonemissive NCs show two strong broad emission bands in the UV spectral region with maxima at 348 nm (3.56 eV) and 404 nm (3.07 eV). The fitting of the high- and low-energy emission spectra as well as band maximum positions as a function of temperature can be found in Figures S3 and S4. As the temperature decreases, the total photoluminescence intensity of these two emission bands increases significantly because of the reduction of nonradiative recombination. While the high-energy emission band shifts continuously toward lower energy as the temperature decreases, the low-energy band shifts toward higher energy.

DOI: 10.1021/acsenergylett.7b01026
ACS Energy Lett. 2017, 2, 2805−2811

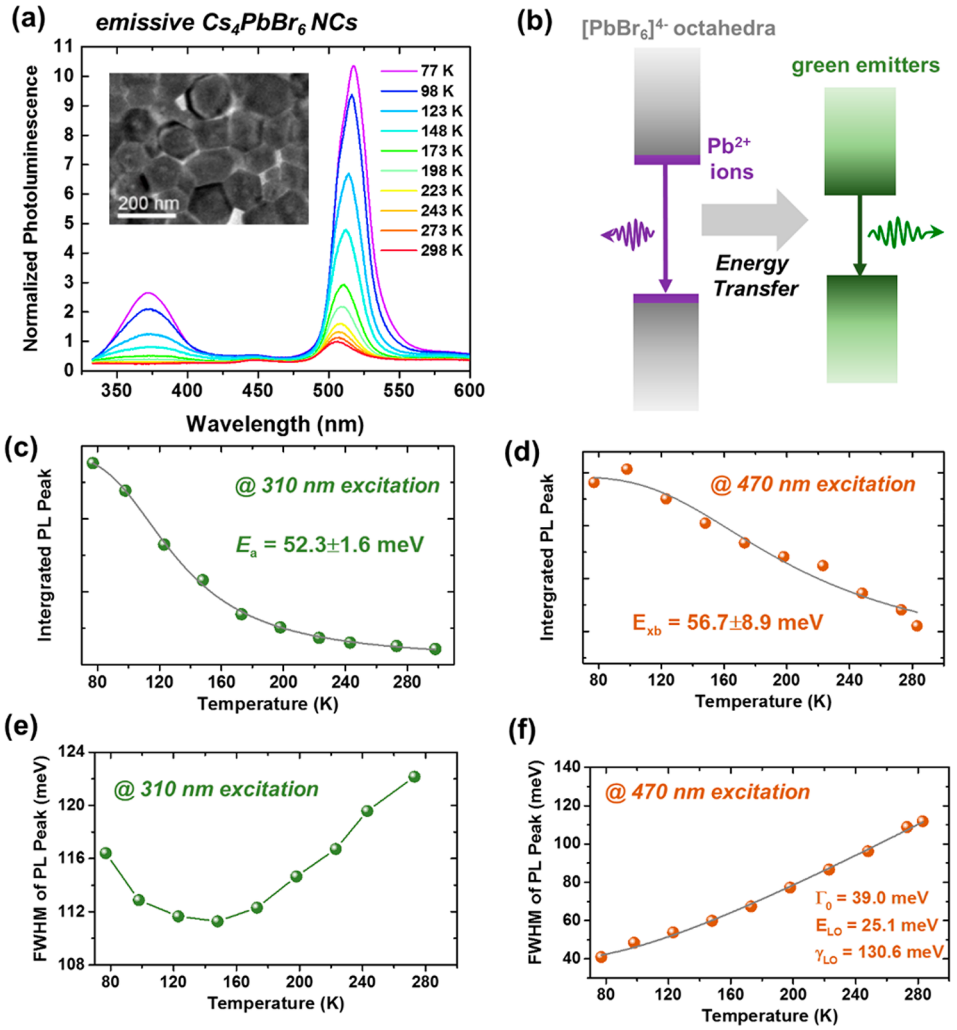

Figure 2. (a) **Temperature-dependent steady-state photoluminescence spectra of emissive Cs_4PbBr_6 NCs together with the TEM image in the inset; (b) diagrammatic sketch of UV and visible emission; (c, d) temperature-dependent integrated PL intensity of green emission using 310 and 470 nm excitations; and (e, f) full width at half-maximum (fwhm) of green emission as a function of temperature using 310 and 470 nm excitations.**

The different shifting behavior suggests that these two emission bands come from different optical transitions related to Pb^{2+} ions that are occupying Cs^+ sites. As illustrated in Figure 1c, the high-energy band is attributed to the allowed optical transition from the excited state ($^3P_1$) to the ground state ($^1S_0$) of the Pb^{2+} ion, which is consistent with previous studies on Pb^{2+} ion emissions in alkaline-earth compounds.[41,42] The $^3P_1$ excited state could be increasingly stabilized by the crystal field as the temperature decreases, leading to the red-shift of the high-energy band. On the other hand, the low-energy band can be assigned to the charge-transfer state (or so-called D-state) emission of the Pb^{2+} ion in the host lattice[41,42] and is due to the strong interaction between Pb^{2+} ions and $[PbBr_6]^{4-}$ octahedra when Pb^{2+} ions occupy Cs^+ sites in Cs_4PbBr_6 NCs. This interaction could be enhanced by the symmetry breaking or distortion of $[PbBr_6]^{4-}$ octahedra due to Jahn–Teller effects (or s^2 ion effects)[43] in the ground state. To confirm the nature of the D-state in the 0D host lattice, we performed density functional theory (DFT) calculations at the GGA/PBE level of theory on Cs_4PbBr_6 supercells before and after Pb^{2+} ion substitution. The optimized crystal structure and band structures along all symmetry k-points of bulk Cs_4PbBr_6 are shown in Figure S5. Cs_4PbBr_6 shows a direct band gap of 3.88 eV at the Γ point, which agrees well with the recently reported experimental band gap of 3.95 eV[29,40] and the value of 3.99 eV calculated at the same level of theory.[40] From the electronic projected density of states (PDOS) of a neutral supercell in Figure 1d, the top valence band is composed of both Br-3p and Pb-6p states, and the bottom conduction band is dominated by the 6p states of Pb.

Once a Cs atom is replaced by a Pb^{2+} ion from the Cs_4PbBr_6 crystal lattice (see Figure 1e), an intragap level (PDOS in red) from this Pb^{2+} ion (D-state) appears close to the conduction band edge. In this case, the excited electron could transfer from a $[PbBr_6]^{4-}$ excited-state level to the D-state of a Pb^{2+} ion, which is achieved through the coupling between D-state and the vibrations of the octahedra in the 0D host lattice (a detailed analysis of the vibrational modes is given later). Therefore, higher temperatures lead to stronger D-state emission from Pb^{2+} ions located in a slightly distorted host environment, in relation to the strong coupling between the D-state and the Pb–Br bond vibrations in the $[PbBr_6]^{4-}$ octahedra. At a low temperature, 77 K, the intensity of D-state emission decreases in favor of the high-energy emission ($^3P_1 \rightarrow {}^1S_0$) because of the

DOI: 10.1021/acsenergylett.7b01026
ACS Energy Lett. 2017, 2, 2805–2811

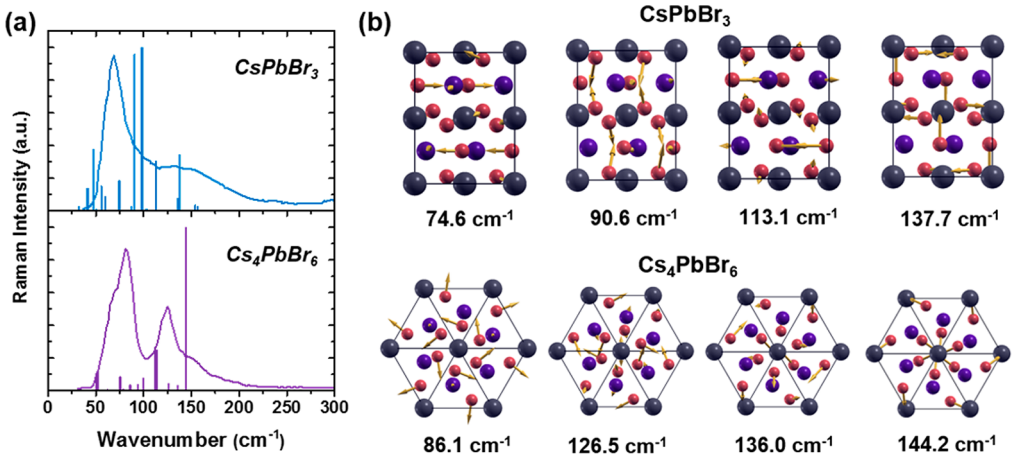

Figure 3. (a) Experimental Raman spectra (gray lines, obtained from ref 49) together with calculated Raman peaks and intensities of $CsPbBr_3$ and Cs_4PbBr_6; (b) their selective vibrational normal modes (the vectors are indicated by yellow arrows).

significant suppression of electron transfer from octahedra to D-states when the coupling becomes weak on the regular crystal lattice sites. Moreover, the D-state emission shifts continuously toward lower energy with increasing temperature because of lattice dilation (i.e., Pb^{2+} ions at Cs+ sites are in the dilated 0D host lattice), which follows the same trend as in typical semiconductors (like Si and GaAs).[44]

We further studied the nonradiative relaxation processes of Cs_4PbBr_6 NCs by fitting the integrated photoluminescence intensities of the two emission bands using the Arrhenius formula: $I = I_0/[1 + a\exp(-E_a/kT)]$, where E_a is the activation energy of the thermal quenching process, k the Boltzmann constant, and I_0 the zero-temperature PL intensity; a represents the strength of the quenching process. As shown in Figure 1b, the extracted activation energies are 37.8 ± 1.9 meV for the high-energy band and 38.4 ± 6.6 meV for the low-energy band; these are consistent with a previous report on Pb^{2+} ions in a Cs_4PbBr_6 thin film (40−43 meV).[29] Because the presence of the charge-compensating vacancy (v_c^-) strongly influences the optical characteristics of Pb^{2+} centers,[45] the activation energy for these emission bands could be ascribed to the localization energy of the exciton to Pb^{2+}−v_c^- luminescent centers as no excess charge related to Pb^{2+} cations exists in the Cs_4PbBr_6 host lattice.

After clarifying the nature of the high-energy luminescence states in nonemissive Cs_4PbBr_6 NCs, we now turn to the photoluminescence properties of emissive Cs_4PbBr_6 NCs containing bright green luminescent centers (see Figure 2a). Similar to the nonemissive Cs_4PbBr_6 NCs, at higher temperatures (180−300 K), the UV emission consists of two broad bands with maxima at approximately 340 and 400 nm (see the enlarged photoluminescence spectra in Figure S6). The former can still be ascribed to the $^3P_1 \rightarrow {}^1S_0$ transition on Pb^{2+} ions and the latter to the D-state emission. As the temperature decreases, the intensity of the latter decreases in favor of the former; once the temperature drops below 180 K, these two emission bands are indistinguishable because of the strong emission overlap. Because the sole broad UV emission band at low temperature is still composed of two emission bands, the proposed fast and slow emissive components in the previous study by Nikl et al.[29] should be associated with the two Pb^{2+} ion emission bands we have described (vide supra).

The strong photoluminescence peak observed in the visible region is consistent with recent reports on emissive Cs_4PbBr_6 NCs,[34,36] where emission was either associated with "3D-like" emitters imbedded in a 0D perovskite matrix[36] or ascribed to crystal structure defects (i.e., Br vacancy).[12,46] As shown in Figure 2c,d, the fitting Arrhenius plots of the integrated photoluminescence intensity using 470 nm excitation gave an activation energy of 56.7 ± 8.9 meV for the green emission (the spectra are shown in Figure S7) and is comparable to the one obtained by 310 nm excitation (E_a = 52.3 ± 1.6 meV). The activation energy for the green emission indicates that there is a thermally activated energy-transfer process from Pb^{2+} ions and $[PbBr_6]^{4-}$ octahedra to the green emission center upon high-energy excitation.

We further analyzed the temperature-dependent emission broadening by extracting the full width at half-maximum (fwhm) of the PL spectra at different temperatures. This method has been used to study the mechanisms of electron−phonon coupling in perovskite materials.[47] In these materials, different scattering mechanisms between charge carriers and phonons or impurities are associated with different functional dependencies of the PL line width $\Gamma(T)$ on temperature and can be expressed as the sum of several contributions:[48]

$$\Gamma(T) = \Gamma_0 + \gamma_{ac}T + \frac{\gamma_{LO}}{e^{E_{LO}/kT-1}} + \gamma_{imp}e^{-E_b/kT}$$

where Γ_0 is the temperature-independent inhomogeneous broadening term; $\gamma_{ac}T$ is the homogeneous broadening term which arises from acoustic phonon scattering through the deformation potential with charge carrier−acoustic phonon coupling strengths of γ_{ac}; the third term is the homogeneous broadening term due to longitudinal optical (LO) phonon scattering with charge carrier−LO phonon coupling strengths of γ_{LO}; the last term is the scattering from ionized impurities with an average binding energy E_b. The acoustic phonons are expected to contribute significantly only in the low-temperature region (T < 60 K).[47] The scattering with ionized impurities does not play a major role in perovskite materials, and the shape of this term could not produce our observed line width variation in Figure 2f. Thus, here, the homogeneous broadening for the green emissions predominantly stems from optical phonons and were investigated by combining Γ_0 and LO phonon−exciton coupling (Γ_{LO}).

As shown in Figure 2f, using 470 nm excitation (below the band gap of Cs_4PbBr_6), the calculated fwhm curve follows the photoluminescence line width broadening by taking into

DOI: 10.1021/acsenergylett.7b01026
ACS Energy Lett. 2017, 2, 2805−2811

account Γ_0 and Γ_{LO}; the fitting values are E_{LO} = 25.1 meV and γ_{LO} = 130.6 meV. Notably, as shown in Figure 2e, the fwhm for visible emission with 310 nm excitation initially decreases with decreasing temperature but increases after the temperature drops below 150 K. This unusual fwhm trend suggests the existence of thermally active energy transfer from Pb^{2+} ions to green luminescent centers using high-energy excitation, as illustrated in Figure 2b. This can also be supported by the observed very weak Pb^{2+} ion emissions in the emissive Cs_4PbBr_6 NCs, especially at high temperatures, as shown in Figure S6. Thus, high-energy photoexcitation of emissive Cs_4PbBr_6 NCs creates electron−hole pairs; then, the recombination of the electron−hole pairs occurs via different pathways, including nonradiative relaxation, Pb^{2+} ion emission, as well as defect-related emission. Here, we propose a model for the defect-related emission: First, trapping of holes occurs at Br vacancies and is followed by the recombination with a shallow trapped electron. This gives rise to the green emission. This assignment also agrees with a recent study of Cs_4PbBr_6 single crystal[12] and microdisks.[46]

To study the phonon modes of 0D perovskites and understand their strong exciton−phonon couplings, we performed DFT calculations of the Raman modes of both $CsPbBr_3$ and Cs_4PbBr_6 (see the computational details in the Experimental Section in the Supporting Information). The experimental Raman spectra of $CsPbBr_3$ and Cs_4PbBr_6 crystals obtained from ref 49 are also shown in Figure 3a for comparison with our calculated spectra. The experimental Raman peaks can be assigned to specific phonon modes by visualizing their calculated vibrational vectors: $CsPbBr_3$ has a strong Raman peak at 72 cm^{-1} (calcd, 74.6 cm^{-1}) and broad band centered at 127 cm^{-1} (calcd, 137.7 cm^{-1}), which can be assigned to the horizontal or vertical Pb−Br stretching modes due to the rigid 3D perovskite structure. For Cs_4PbBr_6, in addition to the Pb−Br stretching modes (exptl, 151.0 cm^{-1}; calcd, 144.2 cm^{-1}), the two strong Raman peaks located at 86.4 cm^{-1} (calcd, 86.1 cm^{-1}) and 126.9 cm^{-1} (calcd, 126.5 cm^{-1}) are attributed to the Pb−Br rocking modes in the $[PbBr_6]^{4-}$ octahedron. All of these modes are attributed to optical phonons because acoustic phonons in perovskite materials have much lower energies (<2.5 meV). On the basis of these results, the Pb^{2+} excitons in the Cs_4PbBr_6 lattice host could predominantly couple to the Pb−Br rocking modes in the $[PbBr_6]^{4-}$ octahedron and result in the D-state emission. On the other hand, this coupling can also promote resonant energy transfer from the $[PbBr_6]^{4-}$ octahedra to the green luminescent centers in the emissive Cs_4PbBr_6 NCs.

In summary, we have studied the photoluminescence properties of Cs_4PbBr_6 nanocrystals that are either nonemissive or emissive in green. In the nonemissive NCs, the two UV emissions are assigned to an optical transition from $^3P_1$ to $^1S_0$ and a D-state in Pb^{2+} ions. The unusual spectral red-shift of $^3P_1$ to $^1S_0$ emission at low temperature is attributed to the stabilization of $^3P_1$ excited state by the crystal field; on the other hand, the blue-shift of D-state emission could be due to 0D crystal lattice dilation. In the emissive NCs, the UV emission has the same origin as in the nonemissive ones, and the resonant energy transfer from $[PbBr_6]^{4-}$ octahedra to green luminescent centers can be largely suppressed by inhibiting the phonon resonance at low temperature. Our work contributes to a better understanding of the Pb^{2+} ion emissions and green luminescent centers in inorganic lead halide perovskites and their derivatives. We suggest that the Pb^{2+} ion emissions can be effectively tuned in the visible spectrum region by adopting different 0D perovskite host lattices.

■ ASSOCIATED CONTENT

Supporting Information

The Supporting Information is available free of charge on the ACS Publications website at DOI: 10.1021/acsenergylett.7b01026.

Experimental and computational details, XRD patterns of nanocrystals, absorption spectra, fitting photoluminescence spectra, and emission band maxima positions; crystal structure and band structure (PDF)

■ AUTHOR INFORMATION

Corresponding Authors

*E-mail: omar.abdelsaboor@kaust.edu.sa.
*E-mail: jean-luc.bredas@chemistry.gatech.edu.

ORCID

Cesare Soci: 0000-0002-0149-9128
Osman M. Bakr: 0000-0002-3428-1002
Jean-Luc Brédas: 0000-0001-7278-4471
Omar F. Mohammed: 0000-0001-8500-1130

Notes

The authors declare no competing financial interest.

■ ACKNOWLEDGMENTS

This work was supported by the King Abdullah University of Science and Technology (KAUST). We acknowledge the IT Research Computing Team and Supercomputing Laboratory at KAUST for their computational and storage resources, as well as their gracious assistance. The work at Georgia Tech has been supported by the Office of Naval Research (Award No. N00014-17-1-2208). C.S. and A.B. acknowledge support from the Ministry of Education (Grant No. MOE2016-T1-1-164) and the National Research Foundation (Grant No. NRF-CRP14-2014-03) of Singapore. We also thank Haoze Yang for assistance in sample preparation and absorption spectra measurements.

■ REFERENCES

(1) De Angelis, F.; Kamat, P. V. Riding the New Wave of Perovskites. *ACS Energy Lett.* **2017**, *2*, 922−923.
(2) Tan, H. R.; Jain, A.; Voznyy, O.; Lan, X. Z.; de Arquer, F. P. G.; Fan, J. Z.; Quintero-Bermudez, R.; Yuan, M. J.; Zhang, B.; Zhao, Y. C.; et al. Efficient and Stable Solution-Processed Planar Perovskite Solar Cells Via Contact Passivation. *Science* **2017**, *355*, 722−726.
(3) Yoon, S. J.; Kuno, M.; Kamat, P. V. Shift Happens. How Halide Ion Defects Influence Photoinduced Segregation in Mixed Halide Perovskites. *ACS Energy Lett.* **2017**, *2*, 1507−1514.
(4) Balakrishnan, S. K.; Kamat, P. V. Au-$CsPbBr_3$ Hybrid Architecture: Anchoring Gold Nanoparticles on Cubic Perovskite Nanocrystals. *ACS Energy Lett.* **2017**, *2*, 88−93.
(5) Murali, B.; Yengel, E.; Yang, C.; Peng, W.; Alarousu, E.; Bakr, O. M.; Mohammed, O. F. The Surface of Hybrid Perovskite Crystals: A Boon or Bane. *ACS Energy Lett.* **2017**, *2*, 846−856.
(6) Murali, B.; Dey, S.; Abdelhady, A. L.; Peng, W.; Alarousu, E.; Kirmani, A. R.; Cho, N. C.; Sarmah, S. P.; Parida, M. R.; Saidaminov, M. I.; et al. Surface Restructuring of Hybrid Perovskite Crystals. *ACS Energy Lett.* **2016**, *1*, 1119−1126.
(7) Chin, X. Y.; Cortecchia, D.; Yin, J.; Bruno, A.; Soci, C. Lead Iodide Perovskite Light-Emitting Field-Effect Transistor. *Nat. Commun.* **2015**, *6*, 7383.

DOI: 10.1021/acsenergylett.7b01026
ACS Energy Lett. 2017, 2, 2805−2811

(8) Tan, Z. K.; Moghaddam, R. S.; Lai, M. L.; Docampo, P.; Higler, R.; Deschler, F.; Price, M.; Sadhanala, A.; Pazos, L. M.; Credgington, D.; et al. Bright Light-Emitting Diodes Based on Organometal Halide Perovskite. *Nat. Nanotechnol.* **2014**, *9*, 687−692.
(9) Saidaminov, M. I.; Mohammed, O. F.; Bakr, O. M. Low-Dimensional-Networked Metal Halide Perovskites: The Next Big Thing. *ACS Energy Lett.* **2017**, *2*, 889−896.
(10) Bakr, O. M.; Mohammed, O. F. Powering up Perovskite Photoresponse. *Science* **2017**, *355*, 1260−1261.
(11) Ahmed, G. H.; Yin, J.; Bose, R.; Sinatra, L.; Alarousu, E.; Yengel, E.; AlYami, N. M.; Saidaminov, M. I.; Zhang, Y.; Hedhili, M. N.; et al. Pyridine-Induced Dimensionality Change in Hybrid Perovskite Nanocrystals. *Chem. Mater.* **2017**, *29*, 4393−4400.
(12) De Bastiani, M.; Dursun, I.; Zhang, Y.; Alshankiti, B. A.; Miao, X.-H.; Yin, J.; Yengel, E.; Alarousu, E.; Turedi, B.; Almutlaq, J. M.; et al. Inside Perovskites: Quantum Luminescence from Bulk Cs_4PbBr_6 Single Crystals. *Chem. Mater.* **2017**, *29*, 7108−7113.
(13) Begum, R.; Parida, M. R.; Abdelhady, A. L.; Murali, B.; Alyami, N. M.; Ahmed, G. H.; Hedhili, M. N.; Bakr, O. M.; Mohammed, O. F. Engineering Interfacial Charge Transfer in $CsPbBr_3$ Perovskite Nanocrystals by Heterovalent Doping. *J. Am. Chem. Soc.* **2017**, *139*, 731−737.
(14) Zhang, D. D.; Eaton, S. W.; Yu, Y.; Dou, L. T.; Yang, P. D. Solution-Phase Synthesis of Cesium Lead Halide Perovskite Nanowires. *J. Am. Chem. Soc.* **2015**, *137*, 9230−9233.
(15) Jellicoe, T. C.; Richter, J. M.; Glass, H. F. J.; Tabachnyk, M.; Brady, R.; Dutton, S. E.; Rao, A.; Friend, R. H.; Credgington, D.; Greenham, N. C.; et al. Synthesis and Optical Properties of Lead-Free Cesium Tin Halide Perovskite Nanocrystals. *J. Am. Chem. Soc.* **2016**, *138*, 2941−2944.
(16) Sarmah, S. P.; Burlakov, V. M.; Yengel, E.; Murali, B.; Alarousu, E.; El-Zohry, A. M.; Yang, C.; Alias, M. S.; Zhumekenov, A. A.; Saidaminov, M. I.; et al. Double Charged Surface Layers in Lead Halide Perovskite Crystals. *Nano Lett.* **2017**, *17*, 2021−2027.
(17) Bisquert, J.; Qi, Y.; Ma, T.; Yan, Y. Advances and Obstacles on Perovskite Solar Cell Research from Material Properties to Photovoltaic Function. *ACS Energy Lett.* **2017**, *2*, 520−523.
(18) Akkerman, Q. A.; Meggiolaro, D.; Dang, Z.; De Angelis, F.; Manna, L. Fluorescent Alloy $CsPb_xMn_{1-x}I_3$ Perovskite Nanocrystals with High Structural and Optical Stability. *ACS Energy Lett.* **2017**, *2*, 2183−2186.
(19) Meinardi, F.; Akkerman, Q. A.; Bruni, F.; Park, S.; Mauri, M.; Dang, Z.; Manna, L.; Brovelli, S. Doped Halide Perovskite Nanocrystals for Reabsorption-Free Luminescent Solar Concentrators. *ACS Energy Lett.* **2017**, *2*, 2368−2377.
(20) Alarousu, E.; El-Zohry, A. M.; Yin, J.; Zhumekenov, A. A.; Yang, C.; Alhabshi, E.; Gereige, I.; AlSaggaf, A.; Malko, A. V.; Bakr, O. M.; et al. Ultralong Radiative States in Hybrid Perovskite Crystals: Compositions for Submillimeter Diffusion Lengths. *J. Phys. Chem. Lett.* **2017**, *8*, 4386−4390.
(21) Peng, W.; Yin, J.; Ho, K. T.; Ouellette, O.; De Bastiani, M.; Murali, B.; El Tall, O.; Shen, C.; Miao, X. H.; Pan, J.; et al. Ultralow Self-Doping in 2D Hybrid Perovskite Single Crystals. *Nano Lett.* **2017**, *17*, 4759−4767.
(22) Cortecchia, D.; Neutzner, S.; Kandada, A. R. S.; Mosconi, E.; Meggiolaro, D.; De Angelis, F.; Soci, C.; Petrozza, A. Broadband Emission in Two-Dimensional Hybrid Perovskites: The Role of Structural Deformation. *J. Am. Chem. Soc.* **2017**, *139*, 39−42.
(23) Yin, J.; Li, H.; Cortecchia, D.; Soci, C.; Brédas, J. L. Excitonic and Polaronic Properties of 2D Hybrid Organic-Inorganic Perovskites. *ACS Energy Lett.* **2017**, *2*, 417−423.
(24) Yuan, Z.; Zhou, C. K.; Tian, Y.; Shu, Y.; Messier, J.; Wang, J. C.; van de Burgt, L. J.; Kountouriotis, K.; Xin, Y.; Holt, E.; et al. One-Dimensional Organic Lead Halide Perovskites with Efficient Bluish White-Light Emission. *Nat. Commun.* **2017**, *8*, 14051.
(25) Saidaminov, M. I.; Almutlaq, J.; Sarmah, S.; Dursun, I.; Zhumekenov, A. A.; Begum, R.; Pan, J.; Cho, N.; Mohammed, O. F.; Bakr, O. M. Pure Cs_4PbBr_6: Highly Luminescent Zero Dimensional Perovskite Solids. *ACS Energy Lett.* **2016**, *1*, 840−845.
(26) Xiao, Z.; Meng, W.; Wang, J.; Mitzi, D. B.; Yan, Y. Searching for Promising New Perovskite-Based Photovoltaic Absorbers: The Importance of Electronic Dimensionality. *Mater. Horiz.* **2017**, *4*, 206−216.
(27) Andrews, R. H.; Clark, S. J.; Donaldson, J. D.; Dewan, J. C.; Silver, J. Solid-State Properties of Materials of the Type-Cs_4MX_6 (Where M = Sn or Pb and X = Cl or Br). *J. Chem. Soc., Dalton Trans.* **1983**, 767−770.
(28) Nikl, M.; Mihokova, E.; Nitsch, K. Photoluminescence and Decay Kinetics of Cs_4PbCl_6 Single-Crystals. *Solid State Commun.* **1992**, *84*, 1089−1092.
(29) Nikl, M.; Mihokova, E.; Nitsch, K.; Somma, F.; Giampaolo, C.; Pazzi, G. P.; Fabeni, P.; Zazubovich, S. Photoluminescence of Cs_4PbBr_6 Crystals and Thin Films. *Chem. Phys. Lett.* **1999**, *306*, 280−284.
(30) Kondo, S.; Amaya, K.; Higuchi, S.; Saito, T.; Asada, H.; Ishikane, M. Fundamental Optical Absorption of Cs_4PbCl_6. *Solid State Commun.* **2001**, *120*, 141−144.
(31) Kondo, S.; Amaya, K.; Saito, T. Localized Optical Absorption in Cs_4PbBr_6. *J. Phys.: Condens. Matter* **2002**, *14*, 2093−2099.
(32) Kondo, S.; Masaki, A.; Saito, T.; Asada, H. Fundamental Optical Absorption of $CsPbI_3$ and Cs_4PbI_6. *Solid State Commun.* **2002**, *124*, 211−214.
(33) Yunakova, O. N.; Miloslavskii, V. K.; Kovalenko, E. N. Exciton Absorption Spectrum of Thin $CsPbI_3$ and Cs_4PbI_6 Films. *Opt. Spectrosc.* **2012**, *112*, 91−96.
(34) Zhang, Y. H.; Saidaminov, M. I.; Dursun, I.; Yang, H. Z.; Murali, B.; Alarousu, E.; Yengel, E.; Alshankiti, B. A.; Bakr, O. M.; Mohammed, O. F. Zero -Dimensional Cs_4PbBr_6 Perovskite Nanocrystals. *J. Phys. Chem. Lett.* **2017**, *8*, 961−965.
(35) Liu, Z. K.; Bekenstein, Y.; Ye, X. C.; Nguyen, S. C.; Swabeck, J.; Zhang, D. D.; Lee, S. T.; Yang, P. D.; Ma, W. L.; Alivisatos, A. P. Ligand Mediated Transformation of Cesium Lead Bromide Perovskite Nanocrystals to Lead Depleted Cs_4PbBr_6 Nanocrystals. *J. Am. Chem. Soc.* **2017**, *139*, 5309−5312.
(36) Quan, L. N.; Quintero-Bermudez, R.; Voznyy, O.; Walters, G.; Jain, A.; Fan, J. Z.; Zheng, X. L.; Yang, Z. Y.; Sargent, E. H. Highly Emissive Green Perovskite Nanocrystals in a Solid State Crystalline Matrix. *Adv. Mater.* **2017**, *29*, 1605945.
(37) Palazon, F.; Almeida, G.; Akkerman, Q. A.; De Trizio, L.; Dang, Z. Y.; Prato, M.; Manna, L. Changing the Dimensionality of Cesium Lead Bromide Nanocrystals by Reversible Postsynthesis Transformations with Amines. *Chem. Mater.* **2017**, *29*, 4167−4171.
(38) Palazon, F.; Urso, C.; De Trizio, L.; Akkerman, Q.; Marras, S.; Locardi, F.; Nelli, I.; Ferretti, M.; Prato, M.; Manna, L. Postsynthesis Transformation of Insulating Cs_4PbBr_6 Nanocrystals into Bright Perovskite $CsPbBr_3$ through Physical and Chemical Extraction of CsBr. *ACS Energy Lett.* **2017**, *2*, 2445−2448.
(39) Yang, H.; Zhang, Y.; Pan, J.; Yin, J.; Bakr, O. M.; Mohammed, O. F. Room-Temperature Engineering of All-Inorganic Perovskite Nanocrsytals with Different Dimensionalities. *Chem. Mater.* **2017**, DOI: 10.1021/acs.chemmater.7b04161.
(40) Akkerman, Q. A.; Park, S.; Radicchi, E.; Nunzi, F.; Mosconi, E.; De Angelis, F.; Brescia, R.; Rastogi, P.; Prato, M.; Manna, L. Nearly Monodisperse Insulator Cs_4PbX_6 (X = Cl, Br, I) Nanocrystals, Their Mixed Halide Compositions, and Their Transformation into $CsPbX_3$ Nanocrystals. *Nano Lett.* **2017**, *17*, 1924−1930.
(41) Folkerts, H. F.; Ghianni, F.; Blasse, G. Search for D-Level Emission of Pb^{2+} in Alkaline-Earth Aluminates and Gallates. *J. Phys. Chem. Solids* **1996**, *57*, 1659−1665.
(42) Folkerts, H. F.; Van Dijken, A.; Blasse, G. Two Types of Luminescence from Pb^{2+} in Alkaline-Earth Fluorohalides with the PbFCl Structure. *J. Phys.: Condens. Matter* **1995**, *7*, 10049−10057.
(43) Sastry, S. B. S.; Viswanathan, V.; Ramasastry, C. Lead Centers in Alkali-Halides - NaCl, KCl and KBr. *J. Phys. Soc. Jpn.* **1973**, *35*, 508−513.
(44) Varshni, Y. P. Temperature Dependence of the Energy Gap in Semiconductors. *Physica* **1967**, *34*, 149−154.

DOI: 10.1021/acsenergylett.7b01026
ACS Energy Lett. 2017, 2, 2805−2811

(45) Zazubovich, S. Polarization Spectroscopy of ns^2 Impurity Ions in Alkali-Halides. *Int. J. Mod. Phys. B* **1994**, *8*, 985−1031.
(46) Seth, S.; Samanta, A. Fluorescent Phase-Pure Zero-Dimensional Perovskite-Related Cs_4PbBr_6 Microdisks: Synthesis and Single-Particle Imaging Study. *J. Phys. Chem. Lett.* **2017**, *8*, 4461−4467.
(47) Wright, A. D.; Verdi, C.; Milot, R. L.; Eperon, G. E.; Perez-Osorio, M. A.; Snaith, H. J.; Giustino, F.; Johnston, M. B.; Herz, L. M. Electron-Phonon Coupling in Hybrid Lead Halide Perovskites. *Nat. Commun.* **2016**, *7*, 11755.
(48) Rudin, S.; Reinecke, T. L.; Segall, B. Temperature-Dependent Exciton Linewidths in Semiconductors. *Phys. Rev. B: Condens. Matter Mater. Phys.* **1990**, *42*, 11218−11231.
(49) Cha, J.-H.; Han, J. H.; Yin, W.; Park, C.; Park, Y.; Ahn, T. K.; Cho, J. H.; Jung, D.-Y. Photoresponse of $CsPbBr_3$ and Cs_4PbBr_6 Perovskite Single Crystals. *J. Phys. Chem. Lett.* **2017**, *8*, 565−570.

DOI: 10.1021/acsenergylett.7b01026
ACS Energy Lett. 2017, 2, 2805−2811